Changes in the mechanical, structural and electrical properties of glassy carbon due to strontium and silver co-implantation and annealing

O.S. Odutemowo[a,*], J.B. Malherbe[a], R. Limbach[b], L. Wondraczek[b], E. Wendler[c], A. Undisz[d], E.G. Njoroge[a], D.O. Idisi[e], M.S. Dhlamini[e]

[a]Department of Physics, University of Pretoria, Pretoria 0002, South Africa
[b]Otto Schott Institute of Materials Research, Chair of Glass Chemistry, Friedrich Schiller University Jena, Jena, Germany
[c]Institute of Solid-state Physics, Friedrich Schiller University Jena, Jena, Germany
[d]Otto Schott Institute of Materials Research, Chair of Metallic Materials, Friedrich Schiller University Jena, Jena, Germany
[e]Department of Physics, College of Science, Engineering and Technology, University of South Africa, Private Bag X6, Florida 1710, South Africa

*Corresponding author. u12052613@tuks.co.za

Abstract

The effect of Sr and Ag co-implantation and recovery annealing on the structural, mechanical and electrical properties of glassy carbon is reported. Glassy carbon was co-implanted with 200 keV Sr and Ag ions to a fluence of 1×10^{16} ions/cm^2 at room temperature. Combination of Raman spectroscopy and high resolution transmission electron microscopy (HRTEM) showed that the co-implantation of Sr and Ag resulted in amorphisation of the glassy carbon substrate. Raman spectra and HRTEM micrographs obtained after annealing indicated recovery of the glassy carbon structure, however, the recovered structure appears to be graphite-like. Instrumented indentation experiments on the ion-irradiated glassy carbon substrates revealed the formation of a surface layer with considerably enhanced mechanical performance. When annealing the ion implanted samples, these effects were only partially reversible. The effect of the irradiation-induced amorphisation and graphitisation of glassy carbon on its conductivity was also studied. The sample became less conductive after Sr and Ag co-implantation, whereby annealing resulted in an increase in conductivity.

Graphical abstract

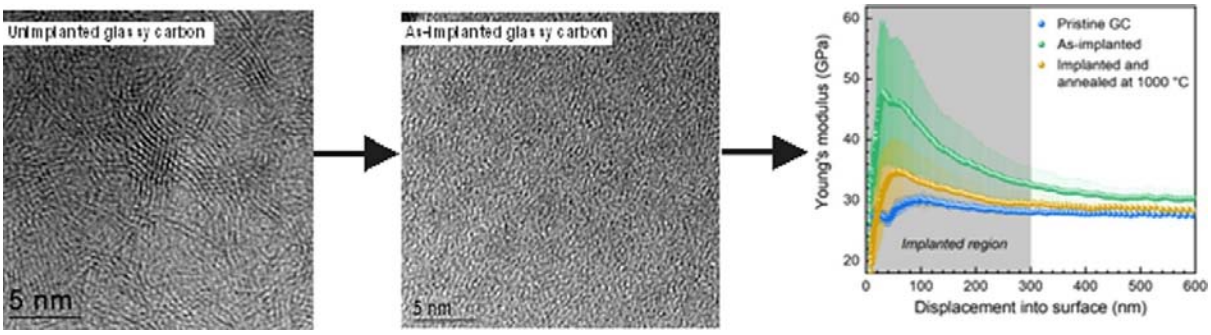

Keywords: Glassy carbon; Ion-implantation; Heat treatment; Nano-hardness; Raman spectroscopy; HRTEM; Electrical characterization

\

1. Introduction

Glassy carbon (also known as vitreous carbon) is a synthetic carbon material favoured for its many present and future applications. This is due to its exceptional ability to retain most of its properties at extremely high temperatures and in a radiation environment. Some of the other properties of glassy carbon that have made it a formidable allotrope of carbon include its high chemical stability and low permeability to gases [1]. These properties led to glassy carbon being an excellent material for, e.g. electrode materials used in electrochemistry or high temperature crucibles.

Glassy carbon is typically produced by the pyrolysis of an organic polymer in a controlled environment. The final product from the pyrolysis process is often heated at temperatures ranging from 1000 to 3000 °C to produce a more chemically pure and stable carbon [2]. A factor which has attracted a lot of attention is the microstructure of glassy carbon. Several studies have suggested that the glassy carbon structure consists of purely sp^2 carbon bonds. However, a fraction of these sp^2 bonds have non-planar fullerene-like structure [3]. These non-planar sp^2 bonds are said to be responsible for the very distinct properties of glassy carbon. While most of the properties of glassy carbon are very attractive for industrial applications, glassy carbon is unsuitable for demanding mechanical applications due to its low fracture stress and toughness compared to other pyro-carbons [2], [4].

Ion implantation is an excellent technique for introducing atoms into solid substrates in a controlled manner. During ion implantation process, the fluence, the implantation energy of the atoms as well as the temperature of the substrate are easily controlled and monitored. Hence, the depth profile and the concentration of the implanted species can be given accurately. The implantation of atoms into a substrate may lead to changes in the structural, mechanical and chemical properties of the substrate. Hence, ion implantation has been used extensively in the semiconductor and other industries to optimize the performance of materials. An example of such application is the implantation of nitrogen in steel to prevent cracks and corrosion [5], [6] Ion implantation was also used to introduce Sr and Ag in a controlled way in glassy carbon for different kinds of investigations [7], [8], [9], [10], [11]

In this study, effects of Sr and Ag co-implantation and heat treatment on the structural, mechanical and electrical properties of glassy carbon have been investigated. Sr and Ag are perfect candidates for this study because their diffusion behaviour in glassy carbon have been previously studied and reported [6], [7], [8], [9], [10], [11] To carry out this study, glassy carbon substrates were co-implanted with Sr and Ag ions at room temperature. The structural changes in glassy carbon were monitored using a combination of Raman spectroscopy and high resolution transmission electron microscopy (HRTEM). Instrumented indentation and current-voltage (I-V) experiments were also carried out to investigate changes in the conductivity, hardness and Young's modulus of glassy carbon induced by Sr and Ag co-implantation as well as after annealing.

2. Experimental procedure

A commercial glassy carbon sample (Sigradur®G, HTW Hochtemperatur-Werkstoffe GmbH) was employed as substrate material in this study. The pristine glassy carbon samples were mechanically polished with 1.0 μm and 0.25 μm diamond suspensions and subsequently cleaned in an ultrasonic bath using a combination of alkaline soap solution, de-ionized water and methanol. The samples were then irradiated with Sr and Ag ions at energies of 200 keV

to a fluence of 1×10^{16} ions/cm^2 at room temperature. The influence of radiation damage on the properties of glassy carbon is important to this study, hence, the flux during implantation was kept at about 10^{13} cm^{-2} s^{-1}. This ensured that the temperature of the glassy carbon substrate did not exceed 50 °C during the implantation process. The implanted samples were cut and annealed in vacuum for 1 h at 500 °C and 1000 °C, respectively. Optical micrographs were recorded on all samples by widefield confocal microscopy (Smartproof 5, Zeiss AG).

The implanted Sr and Ag profiles were determined by Rutherford backscattering spectroscopy (RBS) in a tandem accelerator. 2.5 MeV He^+ ions to a total charge of 14 μC and a scattering angle of 168° were used for analysis. The depth distribution of the implanted ions was obtained by fitting calculated spectra to the measured ones. The depth distribution of the implanted ions was varied until a good agreement between calculated and measured spectra is obtained, thus yielding the depth profiles of Sr and Ag ions. RBS spectra were calculated applying the computer code SIMNRA [12]. To reassign depth values, the density of glassy carbon was taken to be 1.42 g/cm^3 corresponding to 7.12×10^{22} at/cm^3.

The glassy carbon samples for HRTEM were prepared by using the Focused Ion Beam (FIB) technique. A protective layer of platinum was applied to the surface of the sample in order to minimize interaction between the focused Ga-Ion beam and the samples. HRTEM measurements were carried out using a JEM-3010 by JEOL operating at a voltage of 300 kV. High resolution images were recorded in bright field mode. The HRTEM micrographs were obtained at different magnifications for comparison.

The structural changes as a result of silver and strontium ion bombardment and heat treatment were monitored by using a Jobin Yvon T64000 Raman instrument. The apparatus consists of a Raman spectrometer with Ar/Kr mixed gas excitation laser of 514.5 nm wavelength and a light microscope equipped with 10×, 50× and 100× magnification objectives. The 50×objective was used throughout the study in order to ensure uniformity. One of the major problems encountered in Raman studies is sample heating, and in order to avoid this; the laser power was kept at less than 1 mW at the sample.

The impact of strontium and silver co-implantation and annealing with regards to electron mobility was investigated by electrical conductivity measurements at room temperature using a Keithley Pico-ammeter (model 6487). The setup consisted of a two-point probe which acted as a diode junction with a dielectric separation between the terminals. The voltage sweep was carried out within a voltage range of −0.01 to 0.01 while the corresponding current was measured.

Depth profiles of the hardness H and Young's modulus E were recorded by instrumented indentation testing using a nanoindentation platform (G200, KLA Co.) equipped with a three-sided Berkovich diamond tip (Synton-MDP) and operating in the continuous stiffness measurement (CSM) [13]. The tip area function and instruments frame compliance were calibrated prior to the indentation experiments on a silica reference glass (Corning Code 7980, Corning Inc.). To ensure high instrumental resolution at very shallow depths the tip area function of the Berkovich indenter was calibrated based on its equivalent contact radius [14]. On each sample, 20 indents with a maximum penetration depth of 2 μm were created at a constant strain-rate of 0.05 s^{-1}. The resulting load-displacement curves were analysed following the method proposed by Oliver and Pharr [15]. Values of H were derived from the load P divided by the projected contact area of the indenter tip A_c:

$$H = \frac{P}{A_c} \tag{1}$$

and the values of E were calculated from the reduced elastic modulus E_r [16]

$$E = (1 - \nu^2)\left[\frac{1}{E_r} - \frac{1-\nu_i^2}{E_i}\right]^{-1} \tag{2}$$

Here, E_i = 1141 GPa and $\hat{I}½_i = 0.07$ are the elastic constants of the diamond indenter and $\nu = 0.18 \pm 0.01$ is the Poisson's ratio of pristine glassy carbon, as determined by ultrasonic echography using piezoelectric transducers operating at frequencies of 8 – 12 MHz (Echometer 1077, Karl Deutsch GmbH & Co. KG).

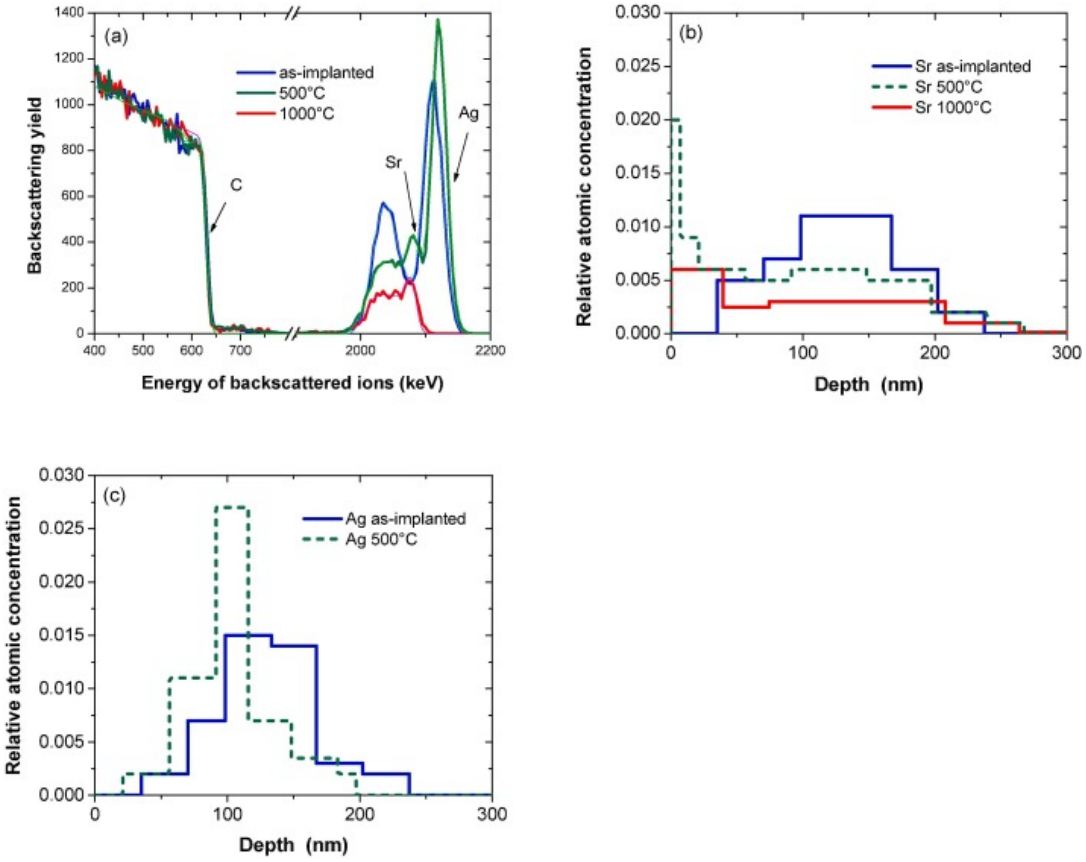

Fig. 1. RBS spectra (a) of 2.5 MeV He ions backscattered on glassy carbon co-implanted with Sr and Ag ions after implantation and after annealing at 500 °C and 1000 °C, respectively. The fitted curves calculated with SIMNRA are given as thin lines. Parts (b) and (c) show the depth distribution of Sr and Ag obtained from the spectra, respectively [1], [2], [3], [4], [5], [6], [7], [8], [9], [10], [11], [12], [13], [14], [15], [16], [17], [18], [19], [20], [21], [22], [23], [24], [25], [26], [27], [28], [29], [30], [31], [32], [33], [34], [35], [36].

3. Results and discussion

3.1. Depth profiles of Sr and Ag atoms obtained from RBS

Results from the RBS analysis after Sr and Ag co-implantation and annealing are shown in Fig. 1. Even though there is a slight overlap of the Sr and Ag signals, reliable profiles can be obtained by fitting the measured spectra as described in Section 2. The profiles shown in Fig. 1(b) and (c) yield an ion fluence of 10^{16} cm^{-2} for each ion species after implantation as well as after annealing at 500 °C in good agreement with the nominal value applied of 1×10^{16} cm^{-2}. The Ag and Sr depth profiles overlap with each other as was planned to ascertain any synergistic effects. During annealing at 500 °C the implanted Sr and Ag atoms were not lost but redistributed within the implanted layer. Ag atoms tended to agglomerate closer to the surface, whereas the Sr distribution flattened in depth and some Sr atoms accumulated at the surface. After annealing at 1000 °C, no Ag atoms were detected by RBS. The Sr signal reduces to about 58% of the original value as was already shown previously [10].

3.2. Structural characterization of the implanted and annealed glassy carbon layers by HRTEM

Fig. 2 shows a cross-sectional bright field HRTEM image of pristine glassy carbon. The sample contains a number of layered graphitic nanostructures with different orientations as can be seen in the figure. Some of these graphitic layers are slightly organized into onion-like features, i.e. imperfect fullerene structures. Embedded around the onion-like features are graphitic-like fringes of various sizes and orientation. The mixture of these features shows that glassy carbon is a highly disordered carbon material with no long-range order.

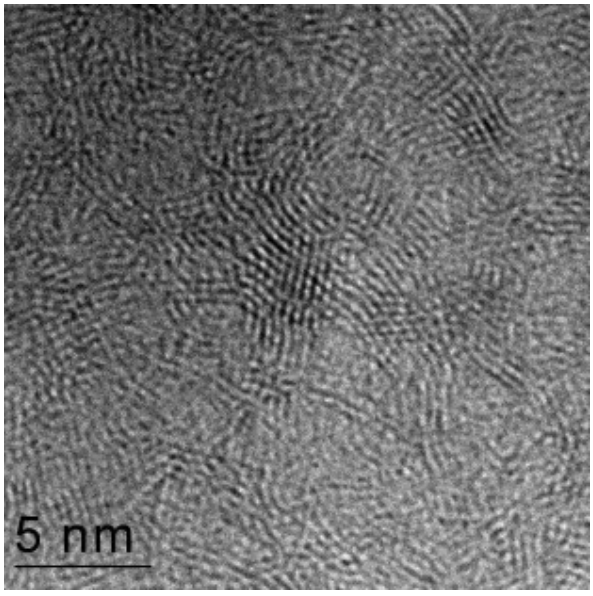

Fig. 2. HRTEM images of pristine glassy carbon. Fig. 2 was extracted from Ref. [7].

Fig. 3 shows HRTEM images obtained at different magnifications of the glassy carbon sample co-implanted with 200 keV Sr and Ag ions to a total fluence of 1×10^{16} ions/cm^2. Fig. 3(a) shows a clear distinction between the implanted near surface region and the bulk of the glassy carbon which is still pristine. The implanted layer is indicated by a red bar. The

thickness of this layer is about 180 nm. This is slightly less than the 200–250 nm obtained from the RBS analysis (see Fig. 1). There are two reasons for this difference. First, smaller depths would be obtained from RBS, if the density of the implanted glassy carbon is larger than that of the pristine material. This indicates a possible compaction of the material during implantation. Second, the result suggests that the glassy carbon retained its original structure at the end of the implanted layer. This may be related to the fact that the energy deposition of the implanted ions in atomic collisions is low in this depth range. Fig. 3(b) shows an image of the implanted layer taken at higher magnification. These TEM images do not reveal any cluster formation of the implanted ions. From Fig. 3(b) one can see that, although there are still graphitic fringes and nano-sized organized structure visible in this image of the implanted layer, they are considerably less and smaller than in pristine glassy carbon. This is an indication of amorphization of glassy carbon upon implantation of Sr and Ag ions, in line with our previous Raman spectroscopic studies [7], [8] which showed that room temperature ion bombardment by heavy ions amorphised the implanted region of glassy carbon. However, as shown in [8] it is still possible to deconvolute the broad Raman band into the typical D and G peaks of glassy carbon. The reason for this can be traced to Fig. 3(b) which shows the existence of some ordered regions in the amorphous layer, albeit significantly less and smaller than in pristine glassy carbon. The thickness of the implanted layer is estimated to be between 200 and 250 nm from the RBS depth profiles shown in Fig. 1(b). The glassy carbon retained its original structure at greater depths. The loss of the slightly organised structure of glassy carbon as a result of ion implantation played a vital role in the changes of the electrical and mechanical properties of glassy carbon as will be discussed below.

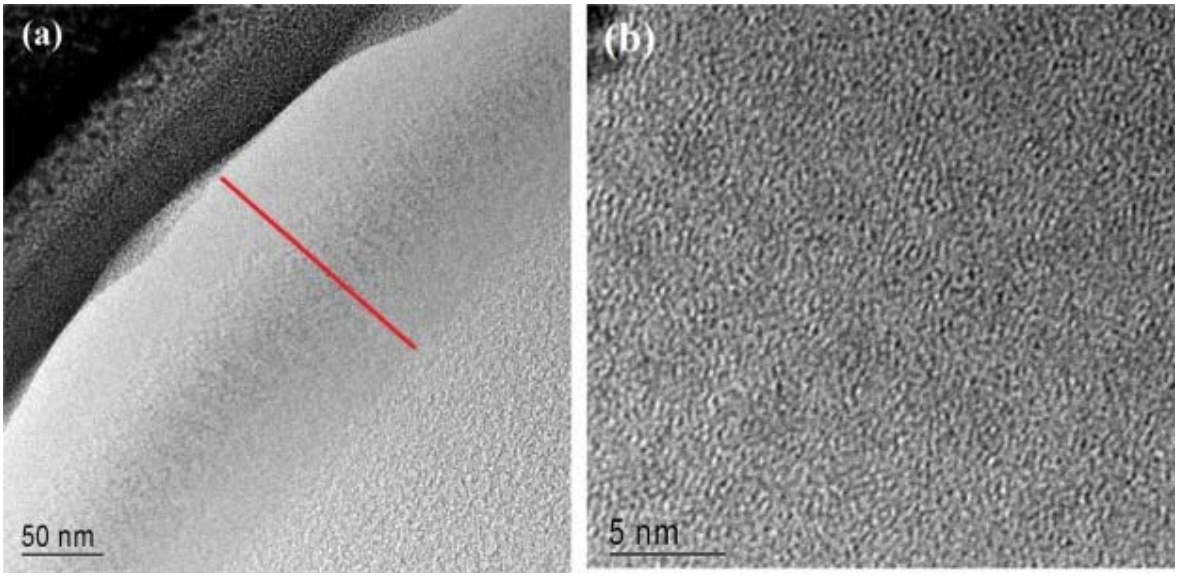

Fig. 3. HRTEM micrographs showing the effect of Sr and Ag co-implantation on the microstructure of glassy carbon. (a) shows the Pt protective layer on the top left corner, the implanted layer (indicated by a red arrow) and the bulk of the glassy carbon, while (b) shows a higher magnification of the implanted layer.

To study the effect of a subsequent heat treatment on the structure of ion irradiated glassy carbon, the Sr and Ag co-implanted sample was annealed in vacuum for 1 h at 500 °C. HRTEM images recorded after annealing are shown in Fig. 4. From Fig. 4(a) it can be seen that a distinction between the implanted near surface region and the bulk of the glassy carbon is still visible after annealing at 500 °C. The thickness of this layer is the same as for the as-

implanted case (see Fig. 3(a)). Fig. 4(c) was taken in the vicinity of the end of ion penetration and is representative of the transition from an amorphous region to a pristine glassy carbon microstructure. Consequently, graphitic fringes are visible in the image. One key feature in the images obtained after heat treatment (labeled (a), (b) and (d)) is the appearance of darker regions within the implanted region of the glassy carbon. They occur at a depth of around 100 nm. This is the depth where especially Ag atoms accumulated after annealing at this temperature (see Fig. 1(c)).

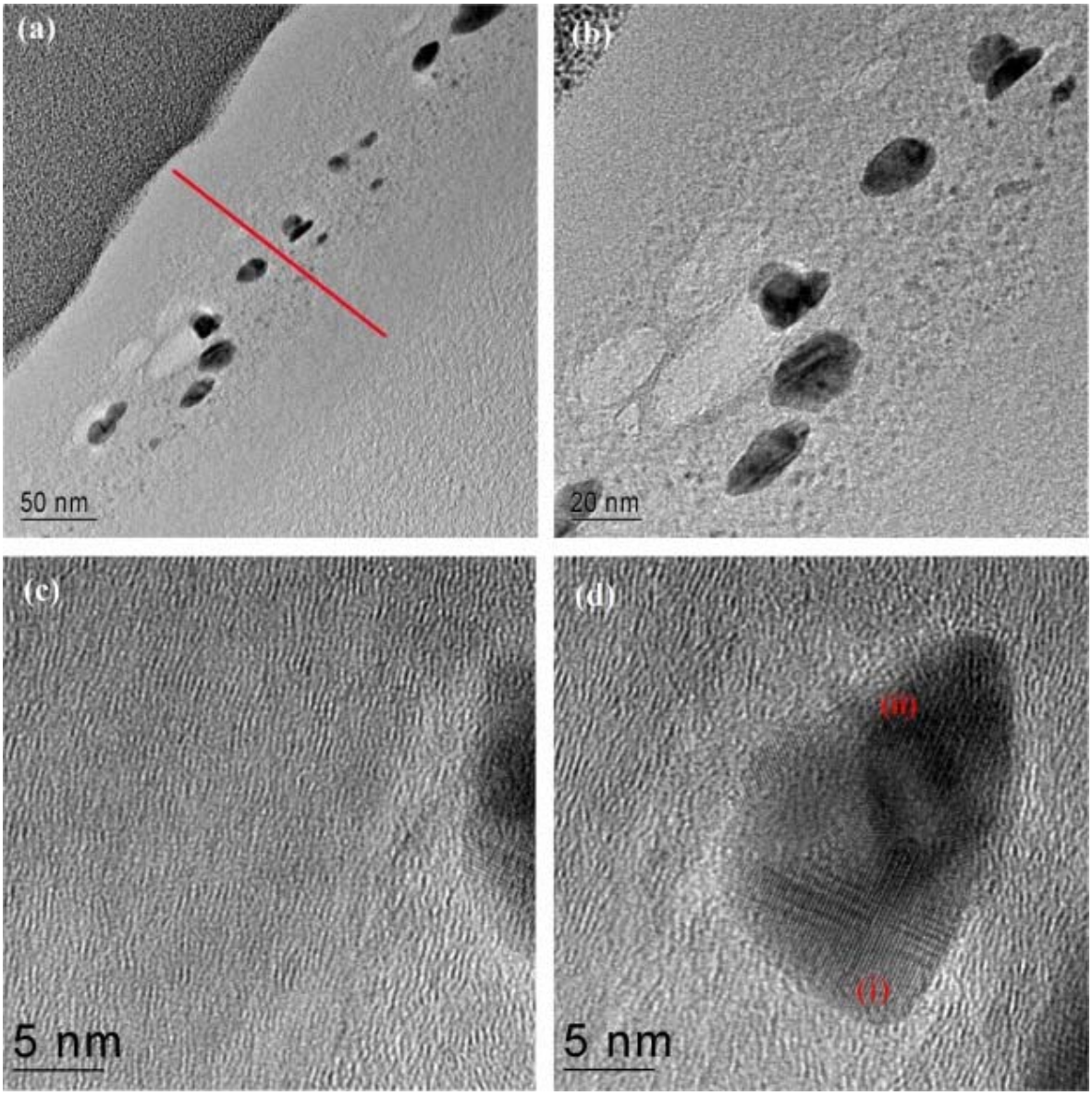

Fig. 4. HRTEM images showing the effect of a heat treatment for 1 h at 500 °C on the nano-structure of Sr and Ag co-implanted glassy carbon. (a) shows the contrast between the Pt protective layer, the implanted layer and the bulk of the glassy carbon substrate. (b) and (c) are HRTEM images obtained within the implanted layer at different magnifications. (c) was taken near the end of range on the ions. (d) shows one of the clusters present within the implanted region at a higher magnification.

To ascertain that the clusters present at depth of approximately 100 nm are indeed Ag atoms, the distances between the fine lines in the nano structure (areas labelled (i) and (ii) in Fig.

4(d)) were measured. For the lower area labelled (i), the distance measured was 0.238 nm while 0.242 nm was measured for the upper left area labelled (ii). The interplanar spacings measured in these regions are approximately comparable to the (111) plane of cubic Ag which is 0.244 nm. This confirms that the agglomerates present after annealing the sample at 500 °C consist of Ag atoms. Another interesting feature of these clusters is that they appear to be composed of poly-crystalline material. This crystallisation is not uncommon when implanted ions conglomerate into clusters near the middle of the implanted region, i.e. in the region of the projected ranges R_p of the two ion species. In this region the concentrations of the implanted ions are greatest. In the TEM image (see Fig. 3) of the as-implanted sample there are also an indication of these clusters but significantly smaller. Annealing allowed some the implanted ions to diffuse into larger clusters. There are plenty such examples in ion implanted SiC and subsequently annealed – see the review by Malherbe [17].

HRTEM shows that annealing the sample at 500 °C resulted in a preferred orientation of graphitic fringes within the implanted region (see Fig. 4(c)). These features were barely visible in the TEM images of the as-implanted region. This suggests a slight recovery of the carbon structure present within the implanted layer. However, the carbon structure recovered appears to be graphite-like compared to the pristine glassy carbon which had onion-like structures.

3.3. Characterisation of implanted and annealed glassy carbon layers by Raman spectroscopy

To ascertain the structural changes in glassy carbon due to Sr and Ag co-implantation as well as the recovery annealing, Raman spectroscopic measurements were carried out on the samples. For the excitation laser line used here, the coefficient of extinction of glassy carbon is between 0.7 and 0.8 [17], [18], [19]. These values are in agreement with an estimation in Ref. [7]. This means that about the upper half of the implanted layer is probed. Fig. 5 shows Raman spectra obtained from the pristine glassy carbon, as–implanted glassy carbon and implanted glassy carbon annealed for 1 h at 500 °C and 1000 °C, respectively. In the spectrum of pristine glassy carbon two distinct first order peaks are clearly discernable. The D peak at around 1350 cm^{-1} is related to the long-range disorder mode of the sp^2 structure while the G peak at around 1585 cm^{-1} is attributed to the in-plane vibration mode of the sp^2 bonds. The first order also shows an additional peak at 1620 cm^{-1}, which is usually denoted as D' and appears in graphitic carbons with small sized of graphite domains [20], [21], [22] Also shown in Fig. 5 is the Raman spectrum of the glassy carbon obtained after implantation. The Raman spectrum shows that the D and G peaks merged into a single broad envelope. This indicates that the implantation of Sr and Ag resulted in the amorphisation of the glassy carbon substrate. The Raman spectra obtained after recovery annealing at 500 °C shows a very slight variation from the as-implanted Raman spectrum, this is due to the slight re-appearance of the G peak. This agrees with the HRTEM results discussed earlier. The spectrum recorded after recovery annealing at 1000 °C exhibited a more pronounced G peak as compared to the spectra of the as-implanted glassy carbon and the sample annealed at 500 °C. This indicates a slight recovery of the glassy carbon structure after annealing at 1000 °C in line with other studies, see for example Ref. [23].

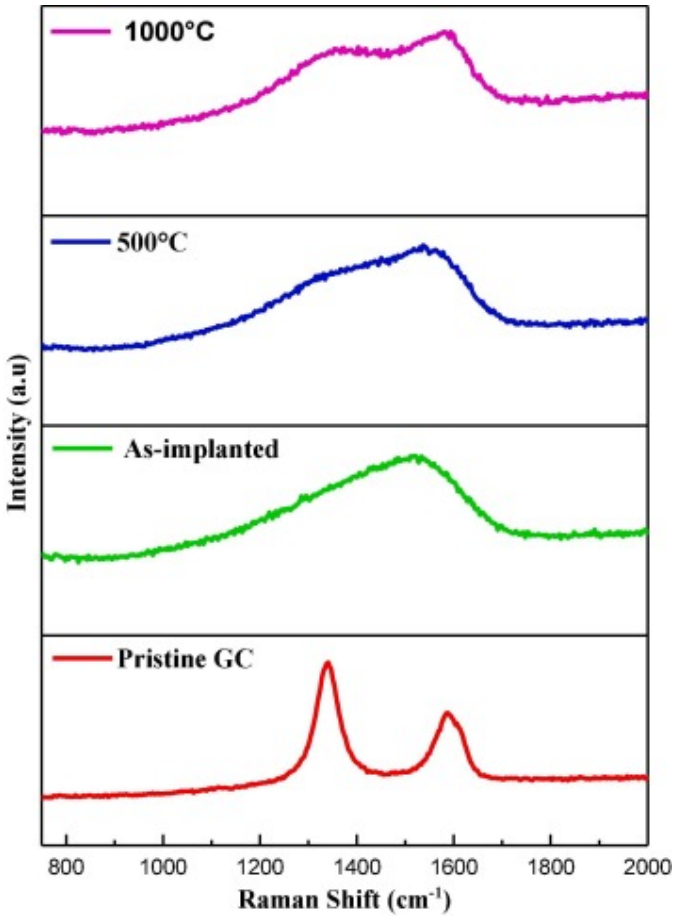

Fig. 5. Raman spectra showing the structural difference between pristine glassy carbon, implanted glassy carbon before and after recovery annealing for 1 h at 500 °C and 1000 °C, respectively.

3.4. Mechanical properties of implanted and annealed glassy carbon layers

The effects of Sr and Ag co-implantation and recovery annealing on the mechanical properties of glassy carbon were studied by instrumented indentation testing. Depth profiles of the Young's modulus and hardness for pristine and as-implanted glassy carbon as well as after annealing for 1 h at 1000 °C are presented in Fig. 6. For pristine glassy carbon (Fig. 6, blue circles), these curves are characterized by an initial increase of E and H with increasing indenter displacement until depth-independent values of $E = 27.4 \pm 0.2$ GPa and $H = 3.81 \pm 0.02$ GPa were achieved at penetration depths of around 150 nm. It is worth noting, that both the Young's modulus and hardness agree very well with the available literature data on glassy carbon [24], [25], [26], [27], [28].

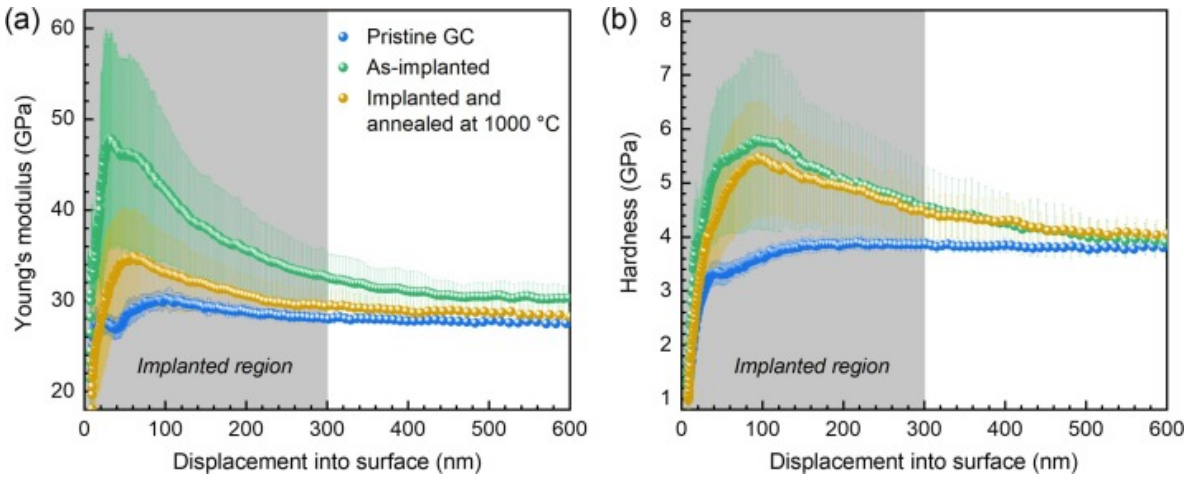

Fig. 6. Effect of Sr and Ag co-implantation and recovery annealing for 1 h at 1000 °C on (a) Young's modulus and (b) hardness of glassy carbon.

The Sr and Ag co-implantation significantly affects the mechanical performance of glassy carbon, as evident from the corresponding depth profiles of the Young's modulus and hardness presented in Fig. 6. The progressive indenter penetration is initially accompanied by a rapid increase in the Young's modulus (Fig. 6(a), green circles) up to a maximum of $E = 47.8 \pm 11.9$ GPa at an indenter displacement of around 31 nm. This is followed by a gradual decrease of E towards the level of pristine glassy carbon as the indentation test proceeds. A comparable trend is seen for the hardness (Fig. 6(b), green circles). After a first increase in hardness up to a maximum of $H = 5.84 \pm 1.68$ GPa at a displacement into surface of around 91 nm, a monotonic decrease of H was noticed with further indenter penetration, eventually approaching the hardness of pristine glassy carbon at indentation depths far below the implanted region (as determined by RBS, see Fig. 1(b), and highlighted with grey shades in Fig. 6). Comparable modifications in the Young's modulus or hardness have previously been reported for glassy carbon irradiated with Ti ions [25]. The enhanced mechanical resistance is a direct consequence of the irradiation-induced amorphisation of glassy carbon, which is accompanied by a permanent compaction (i.e. increase in density) of the material along with a partial conversion of the graphitic-like sp^2 bonds into a kind of sp^3 bonds [7], [29], [30]. Further support for this argumentation is provided by the results of RBS (see Fig. 1(b)) and HRTEM (see Fig. 3(a)). Benefiting from the structural modifications mentioned before, the Young's modulus and hardness of glassy carbon can be raised to about 313 GPa and 26 GPa, respectively, under high hydrostatic pressures of up to 25 GPa [24].

To explain these observations, we refer to the semi-empirical model of Makishima and Mackenzie [31]. Following this concept, the Young's modulus of a glass is determined from the volume density of bond energy and atomic packing density. The latter scales directly with the density. Yet, the degree of densification accessible in glassy carbon by ion implantation [7], [29], [30] or hydrostatic compression [24] may only partially explain the observed changes in Young's modulus. Instead, the increased Young's modulus appears to be controlled primarily by the aforementioned partial conversion of graphitic-like sp^2 bonds into a kind of sp^3 bonds and its effect on the volume density of bond energy. This argumentation also applies for the hardness of ion implanted glassy carbon. The indentation deformation of glasses is basically governed by the competition between elastic deformation, densification and shear-mediated plastic flow. In pristine glassy carbon elastic deformation prevails [24], [25], [26], while densification is supposed to be the dominating mechanism responsible for

the creation of a permanent hardness imprint [26]. The irradiation with ions, however, results in the formation of a densely packed surface layer [7], [25], [29], [30]. Along with the increased Young's modulus, the irradiation-induced compaction may simultaneously also reduce the capacity for an accommodation of the contact stresses through densification during indentation testing. This, in turn, enhances the materials resistance against the penetration of sharp objects as reflected by the significantly improved hardness (Fig. 6(b)).

Annealing the Sr and Ag co-implanted glassy carbon for 1 h at 1000 °C leads to a considerable reduction in Young's modulus (Fig. 6(a)), while the hardness is less affected (Fig. 6(b)). We explain these trends by the slight recovery of the ion implanted glassy carbon structure towards a graphite-like structure upon annealing, as indicated by HRTEM (see Fig. 4(c)) and Raman spectroscopy (see Fig. 5). During this process, sp^3 bonds arising from the preceding irradiation-induced amorphisation of glassy carbon are expected to be converted back (at least partially) to graphite-like sp^2 bonds. As a result, a mechanically more compliant structure is created, which is directly evident from the marked decrease in Young's modulus (Fig. 6(a)). Changes in hardness, on the other hand, are less pronounced since the permanent compaction of the irradiated surface layer (which is assumed to be a key factor for the enhanced resistance against the penetration of sharp objects in ion implanted glassy carbon) retains during the thermal treatment (see Fig. 4(a)).

Although the actual findings on Young's modulus and hardness are well supported by literature, their significance is limited by the relatively large scatter in the experimental data shown in Fig. 6. This is due to the low surface quality of the ion implanted glassy carbon substrates. The pristine glassy carbon exhibits a smooth surface, where the presence of individual surface flaws is only hardly visible (Fig. 7(a)). On the contrary, the existence of numerous scratches, originating from the mechanical polishing, is easily discernible after the irradiation with Sr and Ag ions (Fig. 7(a). During the mechanical polishing process some carbon atoms received enough energy to break the carbon-carbon chemical bonds. These atoms filled up any cavities, such as polishing marks, but remained stuck via van der Waals bonds. While a few of these atoms are removed during the cleaning process, they are mostly (preferentially) sputtered away during the implantation process. The two main factors which determine the sputter yield for a specific ion species are the mass of substrate atoms (which remain constant in this case) and the binding energy of the substrate atom [32]. Since the van der Waals bonded atoms have a significantly lower binding energy than the other chemically bonded carbon atoms they will be preferentially sputtered, thereby revealing the polishing marks.

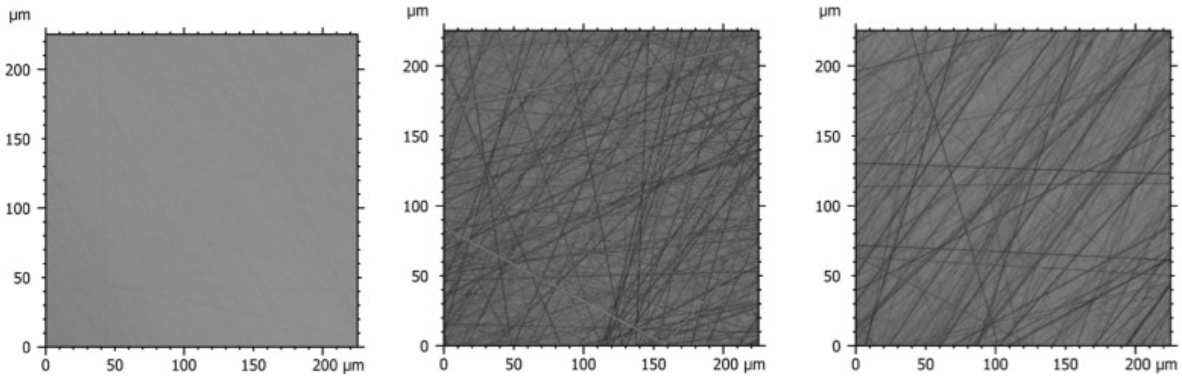

Fig. 7. Optical micrographs of (a) pristine glassy carbon, (b) after Sr and Ag co-implantation and (c) after recovery annealing for 1 h at 1000 °C.

Such pre-existing surface flaws may not only interfere an accurate detection of the materials surface. A rough surface typically also results in poor data reproducibility, particularly, at the initial contact between the indenter tip and the material tested [33].

3.5. Electrical resistance of implanted and annealed glassy carbon layers

The effect of the change in the structure of glassy carbon on its electrical properties is shown in Fig. 8. The I-V characteristic curves are plotted for pristine glassy carbon, after Sr and Ag co-implantation as well as after recovery annealing. The calculated sheet resistance Ω of glassy carbon as a function of implantation and annealing is shown in Table 1. A significant increase in the resistance of the glassy carbon substrate was observed after implantation. After annealing the resistance decreased to a value below that of the pristine material.

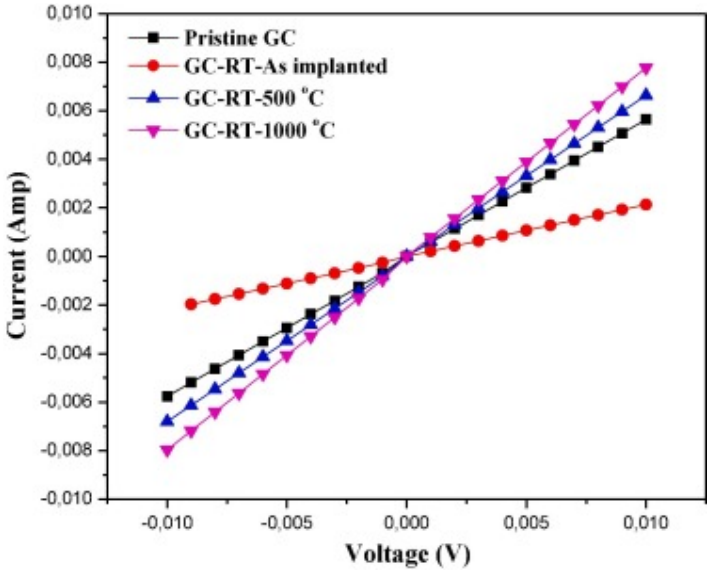

Fig. 8. Changes in the electrical properties of glassy carbon due to Sr and Ag co-implantation and recovery annealing for 1 h at 500 °C and 1000 °C, respectively.

Table 1. Sheet resistance of pristine glassy carbon as well as after Sr and Ag co-implantation and recovery annealing for 1 h at different temperatures.

SAMPLE	RESISTANCE (Ω)
PRISTINE GLASSY CARBON	1.75
AS-IMPLANTED GLASSY CARBON	4.60
500 °C	1.48
1000 °C	1.22

Some studies have been carried out on the electrical conductivity of pristine glassy carbon [34], [35] These studies have shown that there are two main components contributing to the electrical conduction in glassy carbon. These two are normal metallic-type conduction and Mott variable hopping conduction. The latter would occur in the amorphous regions of the glassy carbon. The electrical conductivity σ for this mechanism rapidly decreases with temperature, i.e. $\sigma \propto T^{-4}$, and is much smaller than the metallic component. Metallic conduction would occur in the graphite sheets with percolation between the sheets coupled with hopping conduction. Graphite can be considered as a semi-metal because it is a good

conductor in the basal plane (i.e. *ab*-directions) and an insulator in the *c*-direction. Graphite's highest filled valence band overlaps the lowest empty conduction band by approximately 36 meV [1]. Thus, the delocalized fourth valence electrons form a partially-filled conduction band between the basal planes. The metallic conduction component in glassy carbon is basically independent of temperature and resembles conduction in a metal with strong scattering [34]. Based on the above, one can expect that ion bombardment would significantly increase the resistivity in glassy carbon as it would destruct the nano-graphite sheets in glassy carbon leading to a largely amorphous material as reported above. The electrical conduction would then be based only on variable hopping. Fig. 8 and Table 1 clearly show the significant decrease in conductivity of glassy carbon after ion bombardment.

Raman analysis showed that annealing of bombardment-induced amorphous glassy carbon at various temperatures resulted in a slow recovery of the typical D and G peaks with temperature as shown above and reported in Ref. [8]. The amorphous carbon recrystallised as graphite crystallites. Even vacuum annealing at 2000 °C did not lead to a recovery of the glassy carbon microstructure in the amorphised layer but only to graphite crystallites. Based on the growth of average crystal size with increasing temperature [36], one would expect that the graphite crystallites increased in size with increasing annealing temperature. The temperature-dependent crystal size can qualitatively explain the temperature dependence of the resistance. Increasing the crystal size means that the contribution of metallic conduction to the total conduction would also increase. The fact that the resistance after annealing was lower than for the pristine glassy carbon is an indication that the percolation and hopping components decreased with annealing temperature. The regions with preferred orientation of graphitic fringes, albeit very small after the 500 °C, were probably more in number and nearer to each other than the curved graphite sheets in glassy carbon. Further HRTEM studies are needed to confirm this model.

4. Conclusions

200 keV Sr and Ag co-implantation into glassy carbon was carried out at room temperature. Raman and HRTEM studies showed that the glassy carbon substrate was amorphised after implantation. The amorphisation of glassy carbon due to implantation resulted in significantly improved Young's modulus and hardness, while reducing the conductivity of the material. Raman spectroscopy backed up by the TEM results showed a slight improvement in the structural features of the glassy carbon after annealing. This, in turn, resulted in a loss of the enhanced mechanical performance, as reflected by a substantial drop in Young's and slight decrease in hardness. As opposite to this, an increase in conductivity was observed after annealing the ion implanted glassy carbon at various temperatures. This was attributed to the increase in the sizes and number of graphitic crystallites during the thermal treatment.

CRediT authorship contribution statement

O.S. Odutemowo: Conceptualization, Methodology, Investigation, Writing - original draft. **J.B. Malherbe:** Resources, Writing - review & editing, Supervision. **R. Limbach:** Investigation, Resources, Writing - review & editing. **L. Wondraczek:** Investigation, Resources, Writing - review & editing. **E. Wendler:** Writing - review & editing, Supervision, Funding acquisition. **A. Undisz:** Investigation, Resources, Writing - review & editing. **E.G. Njoroge:** Writing - review & editing. **D.O. Idisi:** Resources. **M.S. Dhlamini:** Writing - review & editing, Supervision.

Declaration of Competing Interest

The authors declare that they have no known competing financial interests or personal relationships that could have appeared to influence the work reported in this paper.

References

1. H.O. Pierson, Handbook of Carbon, Graphite, Diamond and Fullerenes, Noyes Publications, New Jersey, 1993.
2. M. Hassler, Other commonly used biomedical coatings: pyrolytic carbon coatings, Coatings Biomed. Appl. Elsevier, 2012, pp. 75–105.
3. P.J.F. Harris, Fullerene-related structure of commercial glassy carbons, Phil. Mag. 84 (2004) 3159–3167, https://doi.org/10.1080/14786430410001720363.
4. R.O. Ritchie, Fatigue and fracture of pyrolytic carbon: a damage-tolerant approach to structural integrity, J. Heart Valve Dis. 1996 (1996) S9–S31.
5. Q. Wei, Y. Xu, Y. Wang, Textile surface functionalization by physical vapor deposition (PVD), in: Surf. Modif. Text., Elsevier, 2009, pp. 58–90.
6. B. Chico, L. Martinez, F.J. Perez, Nitrogen ion implantation on stainless steel: AFM study of surface modification, Appl. Surf. Sci. 243 (2005) 409–414.
7. O.S. Odutemowo, J.B. Malherbe, L.C. Prinsloo, E.G. Njoroge, R. Erasmus, E. Wendler, A. Undisz, M. Rettenmayr, Structural and surface changes in glassy carbon due to strontium implantation and heat treatment, J. Nucl. Mater. 498 (2018) 103–116, https://doi.org/10.1016/j.jnucmat.2017.10.018.
8. O.S. Odutemowo, J.B. Malherbe, L. Prinsloo, D.F. Langa, E. Wendler, High temperature annealing studies of strontium ion implanted glassy carbon, Nucl. Instrum. Methods Phys. Res. Sect. B Beam Interact. Mater. Atoms. 371 (2016) 332–335, https://doi.org/10.1016/j.nimb.2015.10.054.
9. O.S. Odutemowo, J.B. Malherbe, C.C. Theron, E.G. Njoroge, E. Wendler, IN-SITU RBS studies of strontium implanted glassy carbon, Vacuum 126 (2016) 101–105.
10. O.S. Odutemowo, M.S. Dhlamini, E. Wendler, D.F. Langa, M.Y.A. Ismail, J.B. Malherbe, Effect of heat treatment on the migration behaviour of Sr and Ag CO-implanted in glassy carbon, Vacuum 171 (2020) 109027.
11. D.F. Langa, Diffusion of Implanted Silver and Cesium in Glassy Carbon, University of Pretoria, 2019.
12. M. Mayer, Improved physics in SIMNRA 7, Nucl. Instrum. Methods Phys. Res. Sect. B Beam Interact. Mater. Atoms. 332 (2014) 176–180.
13. R. Limbach, B.P. Rodrigues, L. Wondraczek, Strain-rate sensitivity of glasses, J. Non. Cryst. Solids. 404 (2014) 124–134.
14. D.R. Tadjiev, R.J. Hand, S.A. Hayes, Calibrating a nanoindenter for very shallow depth indentation using equivalent contact radius, Phil. Mag. 90 (2010) 1819–1832.
15. W.C. Oliver, G.M. Pharr, An improved technique for determining hardness and elastic modulus using load and displacement sensing indentation experiments, J. Mater. Res. 7 (1992) 1564–1583.
16. K.L. Johnson, Contact Mechanics, Cambridge Univ, Press, Cambridge, 1985, p. 365.
17. J.B. Malherbe, Diffusion of fission products and radiation damage in SiC, J. Phys. D Appl. Phys. 46 (2013) 473001.
18. L. Pajasova, L. Soukup, L. Jastrabik, D. Chvostova, Optical properties of glassy carbon, Surf. Rev. Lett. 9 (2002) 473–477.
19. M.W. Williams, E.T. Arakawa, Optical properties of glassy carbon from 0 to 82 eV, J. Appl. Phys. 43 (1972) 3460–3463.

20. A.C. Ferrari, J. Robertson, Interpretation of Raman spectra of disordered and amorphous carbon, Phys. Rev. B. 61 (2000) 14095.
21. T. Kozu, M. Yamaguchi, M. Kawaguchi, H. Shima, J.W. Kim, M. Matsuoka, K. Nishida, T. Yamamoto, Evaluating of diamond like carbon using deep UV Raman spectroscopy, Integr. Ferroelectr. 157 (2014) 147–156.
22. T.R. Ravindran, B.R. Jackson, J.V. Badding, UV Raman spectroscopy of single-walled Carbon nanotubes, Chem. Mater. 13 (2001) 4187–4191.
23. J.B. Malherbe, O.S. Odutemowo, C.C. Theron, E. Wendler, Diffusion of strontium implanted glassy carbon, Submitted to Proc. Royal Soc. A.
24. M. Hu, J. He, Z. Zhao, T.A. Strobel, W. Hu, D. Yu, H. Sun, L. Liu, Z. Li, M. Ma, others, Compressed glassy carbon: an ultrastrong and elastic interpenetrating graphene network, Sci. Adv. 3 (2017) e1603213.
25. S. Nakao, K. Saitoh, M. Ikeyama, H. Niwa, S. Tanemura, Y. Miyagawa, S. Miyagawa, P. Jin, T. Bell, L.S. Wielunski, et al., Microindentation measurements of glassy carbon implanted with high-energy titanium ions, Surf. Coatings Technol. 103 (1998) 384–388.
26. M. Sakai, H. Hanyu, M. Inagaki, Indentation-induced contact deformation and damage of glasslike carbon, J. Am. Ceram. Soc. 78 (1995) 1006–1012.
27. K. Jurkiewicz, M. Pawlyta, D. Zygadło, D. Chrobak, S. Duber, R. Wrzalik, A. Ratuszna, A. Burian, Evolution of glassy carbon under heat treatment: correlation structure–mechanical properties, J. Mater. Sci. 53 (2018) 3509–3523.
28. N. Iwashita, M.V. Swain, J.S. Field, N. Ohta, S. Bitoh, Elasto-plastic deformation of glass-like carbons heat-treated at different temperatures, Carbon N. Y. 39 (2001) 1525–1532.
29. D. McCulloch, A. Hoffman, S. Prawer, Ion-beam induced compaction in glassy carbon, J. Appl. Phys. 74 (1993) 135–138.
30. S. Prawer, A. Hoffman, D.G. McCulloch, Structural investigation of xenon ion beam irradiated glassy carbon, Phys. Rev. (1994) 5905–5917.
31. [31] A. Makishima, J.D. Mackenzie, Direct calculation of Young's moidulus of glass, J. Non. Cryst. Solids. 12 (1973) 35–45.
32. J.B. Malherbe, Sputtering of compound semiconductor surfaces. II. Compositional changes and radiation-induced topography and damage, Crit. Rev. Solid State Mater. Sci. 19 (1994) 129–195.
33. J.-Y. Kim, J.-J. Lee, Y.-H. Lee, J. Jang, D. Kwon, Surface roughness effect in instrumented indentation: a simple contact depth model and its verification, J. Mater. Res. 21 (2006) 2975–2978.
34. R.R. Saxena, R.H. Bragg, Electrical conduction in glassy carbon, J. Non. Cryst. Solids. 28 (1978) 45–60.
35. D.F. Baker, R.H. Bragg, The electrical conductivity and Hall effect of glassy carbon, J. Non. Cryst. Solids. 58 (1983) 57–69.
36. C.V. Thompson, Structure evolution during processing of polycrystalline films, Annu. Rev. Mater. Sci. 30 (2000) 159–190.